Detection of Femtomolar Proteins by Non-Fluorescent ZnS Nanocrystal Clusters

*Jingjing Yao, Xiaogang Han, Shang Zeng, and Wenwan Zhong**

Department of Chemistry, University of California, Riverside, California 92521-0403

[*] Corresponding author: Tel: +1-951-827-4952; Fax: +1-951-827-4713.

E-mail address: wenwan.zhong@ucr.edu

Key words: Cation exchange, signal amplification, nanocrystal clusters, porous structure, immunoassay, fluorescence

Abstract

Cation exchange (CX) in the non-fluorescent ZnS nanocrystal clusters (NCCs) was employed to detect trace biomolecules with immunoassays. The NCCs were porous, and allowed fast cation exchange reaction to release an ultra-large number of Zn^{2+} from each cluster that turned on the Zn-responsive dyes for fluorescence detection. The ZnS NCCs were highly stable in biological buffers and more biocompatible than quantum dots. Zn^{2+} release efficiency and target binding by NCCs with average diameters of 44 nm, 86 nm, and 144 nm were investigated. The smallest NCCs exhibited the highest CX efficiency because of its larger surface area and bigger pores inside the cluster structure, and 71.0% of the enclosed Zn^{2+} were freed by CX with 2-minute microwave irradiation. They also experienced the least space hindrance and the fastest rate when binding to target molecules immobilized on surface. When the 44-nm NCCs were used to detect IgE in a sandwich assay, the limit of detection (LOD) was 5 pg/mL (33 fM), 1,000 times better than that of ELISA. Our results well demonstrate that CX in the ZnS NCCs is superior to the conventional signaling strategies in its high amplification efficiency, robustness, and biocompatibility.

Introduction

Ultrasensitive methods for biomolecule detection can benefit diverse areas, including clinical diagnosis[1], biodefense,[2] food quality control[3] and environmental monitoring.[4] The most usual format of sensing is to immobilize the target-recognizing molecules onto the signaling tags that convert each binding event into a measurable signal. Therefore, detection sensitivity is strongly dependent on the capability of the tag in producing large signal increase upon each binding event. Numerous tags of the reporter molecules have been developed, striving to enable detection of rare binding events initiated from trace amounts of targets. Traditional ones include molecules with electrochemical activities,[5] luminescent dyes[6] or complexes[7] with high quantum yields, and enzymes like horseradish peroxidase (HRP).[8,9] Nowadays, a growing number of nanomaterials like metallic nanoparticles,[10,11] carbon nanotubes,[12,13] and quantum dots,[14,15] have been employed to replace these conventional tags. The unique characteristics of nanomaterials, such as ultra-large surface area, superior electronic and optical properties, and readily tailored surface chemistry have greatly boosted the sensitivity and simplicity of molecular detection.[13,16] To further increase the overall signal, amplification has been carried out through encapsulation of thousands of HRP[17,18], quantum dots[19] or organic dyes[20,21] in various types of nanoparticles; or via nucleic acid-based enzymatic reactions.[22,23] Although very low detection limits could be achieved,[23] the complicated reaction designs and inadequate robustness hinder the more general applications in fields like point-of-care diagnosis and on-site biosafety monitoring.

Our group has reported a fast and sensitive signal amplification method that utilizes cation exchange (CX) reaction in nanocrystals (NCs) to release cations from NCs

for ignition of the fluorogenic dyes. Because each NC can encapsulate thousands of cations, a large number of metal-responsive dyes can be triggered by each target-bound NC and emit bright fluorescence for detection of trace amounts of targets.[24-27] The gentle CX reaction involves no strong acids or corrosive oxidants and occurs within a few minutes upon the addition of Ag^+, highly compatible with the common *in vitro* sensing formats.[25-27] Furthermore, higher signal amplification efficiency of CXAmp can be conveniently obtained by encapsulating more metal cations in the nanostructures. Giving that the number of atoms in one spherical or cubical particle is proportional to the cube of its dimension, 10 times increase in particle dimension allows encapsulation of 1,000 times more cations. This means another thousand-fold of signal enhancement is possible with nanoparticles of larger sizes. On the other hand, large NC dimension reduces the surface activity and slows down the CX reaction,[24,28-30] which may not be favorable for CXAmp. To explore the potential of using larger nanostructures in CXAmp, ZnS nanocrystal clusters (NCCs) of different diameters and porosity were synthesized, and their performance in cation release and immunoassay detection was investigated.

Methods

Chemicals and materials

Zinc acetate dihydrate, thiourea, 1-(3-Dimethylaminopropyl)-3-ethylcarbodiimide hydrochloride (EDC), and silver nitrate were purchased from Acros Organics (Pittsburgh, PA). Sulfo-N-hydroxysuccinimide (sulfo-NHS), nitric acid (NF grade) and chemicals used to prepare phosphate-buffered saline (PBS) solutions were purchased from Fisher Scientific. Ethyl alcohol (200 proof) was purchased from Gold Shield Distributors

(Hayward, CA). HEPES, bovine serum albumin (BSA), 2'2-azino-bis(3-ethylbenzothiazdine-6-sulfonic acid) diammonium salt (ABTS), and Tween-20 were obtained from Sigma Aldrich (St. Louis, MO). All of the primary and secondary antibodies with or without biotin modification, streptavidin with or without horseradish peroxide (HRP) modification and FluoZin-3 were from Invitrogen (Carlsbad, CA). The deionized water (DI water) used for preparation of all solutions was produced by the Milli-Q water purification system from Millipore (Billerica, MA).

Synthesis and characterization of ZnS nanocrystal clusters (NCCs)

The ZnS NCCs were synthesized by a hydrothermal approach, using thiourea NH_2CSNH_2 to control cluster growth. In a typical synthesis, 0.8 mmol $Zn(Ac)_2 \cdot 2H_2O$ and 20 mmol thiourea were dissolved in 20 mL DI water to form a clear solution after being stirred for 30 min at room temperature (RT). The solution was then transferred into a stainless steel autoclave (Parr Instrument Co., Moline, IL) with inner Teflon lining (23 mL, Fisher) and maintained at 140 ^oC for 50, 90, and 150 minutes, respectively, in an Isotemp Oven (Fisher). After cooled to RT, the resulting white precipitate was harvested by centrifugation and washed twice with 20 mL DI water and once with 20 mL ethanol. Finally, the particles were dispersed in 1 mL ethanol and kept at 4 ^oC. The aqueous stock cluster solutions used for immunoassay were prepared by washing the clusters with water and redistributing them in 0.02 M phosphate buffer at pH 7.2.

The shape and size of the products were measured using a Philips Tecnai T12 transmission electron microscope (TEM). TEM sample preparation was performed by adding 20 μL of the diluted clusters in ethanol onto a copper grid coated with the

formvar-carbon film (400 meshes, Electron Microscopy Sciences, Hatfield, PA). Subsequently, the sample was dried under vacuum at RT, and imaged in the TEM with operation potential of 120 KV. The Zn content in the cluster was measured by a Perkin-Elmer Optima 2000 DV inductively coupled plasma – atomic emission spectrometer (ICP-AES) (Waltham, MA).

The crystal structure was measured on a Bruker D8 Advance X-ray diffractometer (XRD) with a $Cu_{K\alpha}$ radiation (λ= 1.5418 Å). The data was collected at a scan rate of 0.03 $2\theta°\ S^{-1}$. The Brunauer-Emmett-Teller (BET) surface areas of the powders were determined by a Micromeritics® ASAP 2010 Physisorption Analyzer (Norcross, GA). All samples were degassed at 150 °C prior to nitrogen adsorption measurements. The BET surface areas were determined using a multipoint BET method from the adsorption data in the relative pressure (P/P_0) range of 0.034 – 0.250. The nitrogen desorption volumes at the relative pressure (P/P_0) of 0.977 were used to determine the average pore sizes.

Zn^{2+} release from ZnS NCCs

The zinc cations in the ZnS NCCs were released by three methods: regular CX reaction, CX assisted by microwave and dissolution by nitric acid. Acid dissolution was performed as follows: 208 µL concentrated nitric acid (NF grade, 69-70%, Fisher Scientific) was diluted in 50 mL water (final concentration about 46 mM), and 1 μL ZnS NCCs was added to 100 µl of the diluted nitric acid solution; after the NCCs were dissolved, the solution was neutralized by 10 µL 0.5 N of NaOH and the solution pH was maintained at 7.2 by adding 10 μL of 1.0 M phosphate buffer; finally, 10 μL of 100 mM

HEPES buffer containing 30 μM FluoZin-3 was introduced into the solution for fluorescence measurement. In order to determine the final Zn concentration in the ZnS NCCs solution after acid dissolution, the standard calibration curve was obtained with solutions prepared by the exact same procedure but replacing the 1-μL ZnS NCCs with 1 μL $Zn(Ac)_2$. Cation exchange reaction was performed with a solution containing 500 μM Ag^+ in 1 mM HEPES buffer. If the CX was assisted by microwave digestion, a household microwave oven (Haier, Model: MWM0701TB, New York, NY) was used. Microwave irradiation was performed at a frequency of 2,450 MHz for 2 minutes. After CX, 1 µL of 300 μM FluoZin-3 was added to the CX reaction (final concentration was 3 μM) for Zn quantitation. Fluorescence was measured in the Victor II Microplate reader (Perkin-Elmer, Waltham, MA) using an excitation wavelength filter of 485 nm and an emission filter of 530/30 nm.

Bioconjugation of NCCs

Streptavidin was coupled to the amine-coated ZnS NCCs by EDC and sulfo-NHS. Twenty microliters of the stock ZnS NCCs (~ 2 x 10^{11} particles) were washed with 0.005% Tween-20 solution by centrifugation at 16.1k ×g for 15 min before conjugation. The carboxyl group on streptavidin was activated by mixing 25 μL of 1 mg/mL streptavidin with 6 mg EDC and 5 mg sulfo-NHS dissolved in 1 mL of 20 mM NaH_2PO_4-Na_2HPO_4 (pH 7.2). After activation for 15 min, the residual EDC was quenched by 1 μL 2-mercaptoethanol to prevent protein crosslinking. Then, ZnS NCCs were added to the activated streptavidin and the mixture was gently vortexed for 3 hours at room temperature (RT). At last, the ZnS-streptavidin conjugate was precipitated with

centrifugation at 16.1 ×g for 12 min and re-suspended in 100 μL of 1× PBS. To prepare the anti-IgE-biotin-streptavidin-ZnS complex used in the immunoassay for IgE detection, the streptavidin-ZnS NCCs (~ 2 x 10^{11} particles) were incubated with 40 μL of 0.65 μg/mL goat anti IgE-biotin at RT for 1 hr in 1 mL 1× PBS buffer. The product was washed with 1× PBS and blocked by 4 mL of 5% BSA/PBS solution before being used in the assay. Direct coupling of the goat anti human immunoglobulin G (hIgG) or anti-hIgE to the ZnS clusters was performed with the same procedure, except that 25 μL of 1 mg/mL anti-hIgG or 50 μL of 0.5 mg/mL of anti-hIgE was used.

Immunoassay and fluorescence measurements

The sandwich immunoassay was carried out on a 96-well plate. The wells were coated with 100 μL of 10 μg/mL goat anti-hIgE solutions at 4 ^{o}C overnight and then blocked by 150 μL 5% BSA in PBS buffer for 30 min at RT. The plate was washed three times with 1× PBS. Three rounds of washes with 1× PBS followed with every incubation step in our assay. Afterwards, 100 μL of human IgE at different concentrations were added to the wells and incubated at 4 ^{o}C overnight. Subsequently, the plate was incubated for 4 hrs at RT with 100 μL of the anti-IgE-biotin-streptavidin-ZnS solution. CX was performed in 100 μL solution of 500 μM $AgNO_3$ - 1 mM HEPES, with the entire plate heated in the microwave for 2 min. The reaction solution was cooled to room temperature before 10 μL of 30 μM Fluozin-3 was added to each well to induce fluorescence. For ELISA, the same procedure was applied, except that the anti IgE-biotin was incubated for 3 hr at RT and followed by 1hr incubation with 100 μL of 0.35 μg/mL streptavidin-HRP PBS solution. Color development was carried out in 100 μL of

2 mM H_2O_2 and 2 mM ABTS with 20 min incubation at RT. The green product was measured by the absorbance at 420 nm using the same Victor II Microplate reader.

Effect of cluster size on antibody-antigen binding

The well was completely saturated with 12.9 μg/mL of hIgG solution overnight at 4 ^oC. Then, the goat-anti-hIgG labeled ZnS NCCs were added at concentrations that could cover the entire bottom surface of each well (calculation found in Supporting Information), and incubated at RT for different duration, i.e., 0.5, 1, 2, 3, 4 and 5 hrs. Nitric acid was used to fully digest the bound ZnS NCCs. After neutralization with NaOH, the detection solutions were diluted 400 times before the addition of FluoZin-3 to ensure the Zn^{2+} concentration within the linear detection range. Because the fluorescence was proportional to the total number of bound clusters, the binding rate curve was obtained by plotting the number of the bound ZnS cluster vs. the incubation time.

Note: All standard deviations reported in the figures in form of error bar were obtained from triplicate measurements.

Results and Discussions

NCCs characterization

ZnS NCCs of semi-hollow core-shell structures were synthesized through a simple hydrothermal reaction between zinc acetate dihydrate and thiourea.[31] During the

reaction, small ZnS crystals spontaneously self-assemble into large clusters in order to minimize their interfacial energy. The assembly would result in pores within the cluster structure. The exterior of the clusters should be packed much looser than the interior, because the inner cores are formed under the initial high super-saturation condition which results in a faster nucleation rate.[31,32] The porous structure and loose packing of small crystals could allow faster cation exchange on NCCs.

Indeed, TEM images obtained from our particles (Figure S1) confirmed that, regardless of the particle size, each spherical particle was a cluster of many smaller crystallites, and the outer rim displayed lighter density than the inner core.[31] Heating durations of 50, 90, and 150 minutes produced particles of different diameters as listed in Table 1, with the longest heating time yielding the largest particle diameter. All clusters exhibited the same XRD patterns (Supporting Information Figure S2), with the main diffraction peaks found to be the (002), (110) and (112) peaks of the pure hexagonal phase of ZnS (JCPDS 36-1450). The (100) and (101) peaks overlapped with the (002) peak because of the peak broadening of (002), typical for small crystallites. Based on the Debye-Scherrer formula, the average crystallite size is inversely proportional to the full width of the half maximum peak height. Thus, the broader peak (002) in the 44-nm cluster indicated that it had a smaller crystallite size than the other two clusters. BET test was carried out to determine the surface area and pore diameter (Table 1), and the BET plots were shown in Supporting Information Figure S3. The smallest cluster had the largest relative surface area, and the surface area decreased when the cluster diameter increased. The largest cluster also possessed the smallest pore size, due to the extended heating duration.

Furthermore, the total zinc content of the NCC was quantified by ICP-AES. Quantification of zinc content in clusters and in solution is important for us to evaluate the stability of NCCs in solutions and to calculate the cation release efficiency. Since ICP-AES consumes more than 3 mL of the NCC solution for each measurement, and our instrument offers a detection limit of ony 200 nM for Zn^{2+}, we tested the possibility of using FluoZin-3 for Zn content quantification in our assays, which consumed much smaller solution volumes and offered higher sensitivity and could detect as low as 10 nM Zn^{2+}. During the measurement, NCCs were dissolved in nitric acid. After the pH was neutralized by NaOH and stabilized by phosphate salt, 3 μM FluoZin-3 was added to quantify Zn^{2+}. As shown in Supporting Information (SI) (Table S1), both methods yielded the same NCC stock concentrations, with the ratio of $[Zn^{2+}]_{fluorescence}$ / $[Zn^{2+}]_{ICP}$ ranging from 0.95 to 1.05. Thus, in the following study, the Zn content in solution was quantified with the above procedure by fluorescence.

Zn^{2+} release performance

A solid ZnS sphere with a diameter of 44 nm could encapsulate over 10^6 Zn atoms in each particle, calculated from the density of ZnS and the volume of particle. Even though the NCCs were porous and contained less Zn than solid particles, they should allow efficient CX and give out large signal intensity by releasing a majority of Zn content. We compared the performance of three methods: acid dissolution,[33] CX, and microwave assisted CX. The dissolved Zn^{2+} concentration was obtained from fluorescent measurement, and plotted against the total $[Zn^{2+}]$ in the cluster solution (Figure 1). The

slope of the correlation curve represents the average percentage of Zn^{2+} released from each type of cluster.

Figure 1a clearly showed that nitric acid completely dissolved the ZnS NCCs and the dissolution was independent of the size of NCCs, because the curves for all NCCs had slopes close to 1. However, in order to generate reliable fluorescent signals with the released cations, tedious steps were needed to maintain a stable neutral pH. It was reported that with the saturating Zn^{2+} concentration at 5 μM, FluoZin-3 gave out stable fluorescence from pH 6 to 9, and no fluorescence was observed at pH below 4.[34] Since we were interested in using FluoZin-3 to illuminate the Zn released from the NCCs present at low concentrations, we tested the signal of FluoZin-3 at different pH values with Zn concentration increasing from 100 nM to 1 μM. Indeed, no or very low fluorescence was seen at pH 3 or 4, and the fluorescence intensity at pH 5 and 6 were lower than that at pH 7, even though the signal was stable (Supporting Information Figure S4). This result indicated that fluctuation in pH could bring in variation in fluorescent intensity and could reduce the reproducibility in measurement. In addition, Ag^{+} needed to trigger the cation exchange reaction would be in the detection solution and could increase the instability of the solution pH. Thus, to obtain the neutral pH, the acid dissolution approach involved the following four steps, which were also described in details in the Experimental section: 1) the ZnS NCCs were firstly dissolved by the concentrated nitric acid; 2) then, the solution was neutralized by NaOH; 3) next, an aliquot of 1.0 M phosphate buffer was added to maintain the solution pH at 7.2; 4) finally, the detection solution of 100 mM HEPES with 30 μM FluoZin-3 was introduced into the solution for fluorescence measurement. The HEPES buffer in the detection

solution can mask the interfering cations present in the solution and reduce fluorescence background, and the phosphate buffer was needed to bring in high enough buffer capacity to maintain a stable pH during detection. The multi-step operation maintained a stable pH, but still large variation in the final signal, i.e. large error bars were shown in Figure 1a), due to the manual liquid handling that decreased measurement reproducibility.

Therefore, we continued to test the release performance of the gentler and more convenient cation exchange reaction. With the addition of Ag^+, 42.3 % Zn was released from the 44-nm cluster, but only a small portion of Zn, ~16.6 %, was exchanged out by Ag^+ from the 86-nm clusters (Figure 1b). The largest cluster, due to the extremely small pore size, had the poorest release performance: only about 3.2% Zn was released by CX. This result supported that the porous structure permitted more freedom for the diffusion of Ag^+ and Zn^{2+} inside the nanoparticle structure, and thus rapid CX could occur. With a smaller pore size, only the Zn locating on the particle surface could be freed by CX, but Ag^+ could not penetrate deep enough to release Zn from the interior structure.

To further enhance the release efficiency, we employed microwave irradiation to assist CX. Microwave oven usually works at 2450 MHz to generate intensified, rapid and uniform heating.[35] The heating can greatly affect a reaction system by considerably reducing reaction time and increasing product output. Thus, microwave has been utilized to improve synthesis of organic or inorganic materials,[36-38] and also to enhance sample preparation for analytical operations.[35,39,40] Additionally, microwave is safe and also programmable to accommodate different temperature requirements. It can work with homogeneous or heterogeneous solids or solutions. All these features of microwave make it an attractive method to help with crystal dissolution and improve cation release

from the large NCCs. We found that microwave irradiation for only two minutes led to significant improvement in the percentage of cation release. As shown in Figure 1c, the release percentage increased to 71.0 % and 48.2 % for the 44- and 86-nm clusters, respectively. However, not much improvement was observed with the 144-nm clusters.

Elongated digestion duration is often employed in microwave-assisted digestion of solid samples. We evaluated how the irradiation duration could affect the cation release efficiency. Though, only very subtle enhancement in Zn release was observed, as shown in Supporting Information Figure S5. Similar negligible effect to the product yield from time has also been reported in microwave-assisted nanomaterials preparation.[41] The not-so-significant improvement in CX efficiency obtained with extended digestion time is probably due to the incapability of Ag^+ in penetration through the thick cluster: no matter how long the irradiation lasted, only the outside shells were decomposed. The decomposition was more likely to be assisted by the rapid movement of Ag^+ and the FluoZin-3 dye than the thermal effect. This conclusion could also be supported from the thermodynamic changes of the CX reaction. The enthalpy change ($\Delta_{rxn}H^o_{m,298K}$) of the reaction ($ZnS + 2Ag^+ = Zn^{2+} + Ag_2S$) is calculated to be -205.01 kJ [Note]. Therefore, the CX reaction releases heat and high temperature is not favorable in moving the reaction forward. (**Note**: enthalpy calculation is based on the following values: $\Delta_fH^o_{m,298K,ZnS}$ = -192.63 kJ, $\Delta_fH^o_{m,298K,Ag+,aq}$ = 105.579 kJ, $\Delta_fH^o_{m,298K,Ag2S}$ = -32.59 kJ, and $\Delta_fH^o_{m,298K,Zn2+,\ aq}$ = -153.89 kJ, adopted from Physical chemistry, 3rd edition, Robert G. Mortimer (Burlington, MA), 2008, 1211-1224)

CX and microwave-assisted CX involved only one step, the addition of the detection buffer, and thus were more convenient and reproducible than acid dissolution

when coupled with fluorescence detection. The two CX approaches also generated lower background that led to higher signal-to-noise ratios. The fluorescence amplification ratios (F_R), i.e. the signal intensity to background ratio, of all three cation release methods were compared (Supporting Information Figure S5). Acid dissolution only showed significant improvement in F_R in the 144-nm clusters, which in fact had the lowest F_R value in general among the three types of clusters. The lower F_R can be attributed to the elevated background in the acid dissolution solution due to Zn contamination introduced by the chemicals used in pH neutralization.

Because the microwave-assisted CX yielded similar signal amplification ratios as the acid dissolution approach with much simpler operation, it was selected as the cation-release method in immunoassays employing the ZnS clusters.

Size effect on binding to target

When the size of the reporter tag gets bigger, binding between the labeled reporter antibody and the target could be hindered by steric hindrance. To probe such an effect in clusters, we saturated the bottom of the microtiter plate well with human IgG (hIgG) by overnight incubation with 12.9 μg/mL hIgG at 4 ^{o}C, and then tested the total number of anti-hIgG-conjugated NCCs bound on the surface with the incubation time of 0.5, 1, 2, 3, 4 and 5 hrs. The total amount of NCCs used was also high enough to cover the entire array surface (calculation shown in Supporting Information). With a fixed number of target molecules on surface, the clusters that experience the largest steric hindrance in binding would result in the smallest number of bound NCCs. In order to estimate the total amounts of the bound ZnS clusters, we released all the Zn^{2+} with nitric

acid dissolution and quantified the Zn content by standard zinc solutions. Then we calculated the number of ZnS clusters using the total number of zinc atoms enclosed in one solid ZnS nanoparticle. Because our clusters were porous and should contain less zinc than the solid particles, the calculated number should be lower than the actual ZnS cluster number attached to the bottom of the well. We plotted these numbers versus the incubation time (Figure 2), and found out that the number of the surface-bound 44-nm ZnS clusters increased linearly with the incubation time, and plateaued after 5 hours of incubation at 13.0 fmol. This rate curve indicates that the binding was a zeroth-order reaction, because the amount of adsorbed antigen was fixed and the antibody was added at a saturated concentration. However, for the two larger clusters, after 1-hr incubation, increase of the total numbers of surface bound NCCs started to slow down or even reached saturation. A total of 2.9 and 1.0 fmol of the 86- and 144-nm clusters could be adsorbed onto the plate surface, respectively, much lower than the total number of the 44-nm clusters. Diffusion of the larger clusters to the surface was more difficult than the smaller one, and depletion of antibody concentration in the liquid-solid interface greatly reduced the binding speed, yielding the much lower number of bound clusters.[42] Further, the cluster with a large diameter could block the adjacent binding sites and prevent more clusters to be attached.

The slower diffusion rate of the larger clusters and the higher steric hindrance they experienced when binding to the target delivered poorer detection performance of the larger NCCs (Supporting Information Figure S6). With IgG concentration increasing from 0.5 to 10 ng/mL, fluorescence intensity from the 44-nm NCCs conjugated with anti-hIgG increased faster than that from the 86-nm NCCs, offering higher sensitivity in

detection. The largest cluster did not even show consistent increase in signal, and was harder to be freely dispersed in solution during incubation. Frequent shaking was necessary to keep them from precipitation.

From the above comparison, the clusters with an average diameter of 44 nm were chosen in the following sandwich assay for IgE detection.

Application in sandwich assay for detection of IgE

To demonstrate the power of CXAmp with ZnS NCCs in biomolecules detection, we employed it to analyze human IgE (hIgE) in a sandwich assay format by conjugating the NCCs with streptavidin (Figure 3). IgE is an antibody subclass, found only in mammals. As the least abundant immunoglobulin isotype, IgE can trigger the most powerful immune response. Thus, rapid and accurate detection of IgE is of great importance for timely diagnosis of allergy-mediated disorders. In addition, we had applied the ZnSe NCs-based CXAmp for detection of IgE,[26] and using the same target could facilitate fair performance comparison of the small NCs and the large NCCs. We linked the NCCs with streptavidin (S) and then coupled the biotinylated (B) anti-hIgE to ZnS (ZnS-SB-anti-hIgE). The streptavidin-biotin linkage was to prevent steric interference to antigen binding induced by the relatively large cluster, as well as damage to the binding epitope by the crosslinking chemistry.

Before we applied the 44-nm NCCs in immunoassays, we first examined if they were stable enough for immunoassay and long-term storage. Zn^{2+} released to the solution when stored in 0.02 M phosphate buffer at pH 7.2 for a month was measured by the fluorescence method mentioned above, after the clusters were removed by

centrifugation. The storage solution was sampled every week. We also evaluated the stability of the streptavidin-conjugated 44-nm NCCs when suspended in 1×PBS and sampled every one hour. Both the Zn contents in the supernatant and in the NCCs were quantified; and no Zn^{2+} was detected in the solution when the NCCs were present either in the storage buffer for up to a month or in 1×PBS for 5 hours (Supporting Information Figure S7), showing adequate stability for being used as labeling tags in immunoassays.

It turned out that the ZnS-SB-anti-hIgE complex could detect as low as 5 pg/mL (33 fM) IgE, using the biotinylated anti-IgE (Figure 4a). Even though this assay format required one more incubation step than directly coupling antiIgE to ZnS, it delivered better linearity and reproducibility when detecting trace target molecules. Using the ZnS-SB-antiIgE, the fluorescence intensity increased steadily with the target concentration. On the contrary, the ZnS clusters coupled to antiIgE without the linkage of streptavidin and biotin (ZnS-antiIgE) only gave out marginal signal difference (worse linearity) with large standard deviations (poorer reproducibility) at the three lowest IgE concentrations. Such a difference could be attributed to the high freedom of the antiIgE molecules when coupled to ZnS via the long streptavidin-biotin linkage that reduced the space hindrance during interaction with the target IgE. Moreover, protein-protein crosslinking might have occurred when coupling antiIgE to ZnS, and damaged the binding site of antiIgE to IgE. Streptavidin is more sustainable to harsh conjugation conditions than antibodies, because it is a tetramer and each of the four subunits binds to biotin with equal affinity. Further optimization of the conjugation condition for preparation of ZnS-antiIgE may improve its performance in the simpler assay format, which can be investigated in the future.

In order to efficiently capture very low amounts of IgE, we coated the microtiter plate with 10 μg/mL anti-hIgE. We found out that if the capture antibody concentration reduced by 2 or 10 times, the detection limit increased to 0.01 or 0.1 ng/mL, respectively (Supporting Information Figure S8). Although higher background signals were observed with 10 μg/mL capture antibody, lower detection limit and higher assay reproducibility was obtained. This is because with the extremely low target concentrations, excess capture antibody on the array surface could effectively drive forward the formation of the antibody-antigen complex and give superior sensing performance. As described in the Experimental section, we employed overnight incubation for immobilization of the capture antibody and then the antigen. The long incubation time was necessary to obtain the low detection limit due to the slow diffusion rate of the trace protein molecules to the surface of the well bottom.[43,44] Faster reaction kinetics could be obtained by maximizing the array surface to solution volume ratio with the employment of microfluidic devices. In the case of using the traditional microtiter plate, the only way to solve the diffusion challenge was to increase the incubation time. Moreover, the total number of the ZnS-SB-antiIgE NCCs used was optimized (Supporting Information Figure S9). Raising the total number of NCCs from 1×10^9 to 5×10^9 resulted in a larger dynamic range as well as better sensitivity, but 1×10^{10} NCCs significantly increased the background signal. The final assay then employed a total of 5×10^9 NCCs for the detection of IgE.

The linear regression curve for detection with the ZnS-SB-anti-hIgE NCCs was shown in Figure 4a with a a limit of detection (LOD) of 5 pg/mL IgE and a linear range spanning up to 100 pg/mL. Beyond the linear range, the fluorescence intensity still increased steadily with IgE concentration (Supporting Information Figure S10). The

fluorescence vs. concentration curve holds the form of Langmuir isotherm and leveled off at 10 ng/mL IgE, indicating saturation of all binding sites on the array surface. We reported previously that CXAmp with the small, 5-nm ZnSe nanocrystals (NCs) could detect as low as 1 ng/mL IgE in standard solutions. Now using CXAmp with the ZnS NCCs, 200-fold improvement in LOD was obtained.

The detection performance of ZnS NCC-based CXAmp is also much superior to that of the enzyme-linked immunosorbent assay (ELISA). For fair comparison, streptavidin was tagged with horseradish peroxidase (HRP) so that the exact same incubation steps were carried out. The amplification efficiency of both labeling methods was represented by the relative change of signal over background and plotted against IgE concentration in Figure 4b. Besides the steeper slope of the detection curve, i.e. higher sensitivity, CXAmp with ZnS-SB-anti-hIgE NCCs offered a detection limit that is one thousand fold lower: ELISA with horse radish peroxidase could only detect 5 ng/mL IgE.

Conclusion

We reported the development of cation exchange-based signal amplification with ZnS NCCs and its application in immunoassay for detection of human IgE. ZnS NCCs bring in several advantages to immunoassays compared to the smaller ZnSe NCs used in our previous work. The higher amount of Zn^{2+} in the NCC compared to a single crystal delivered 200 fold improvements in detection limit. As low as 5 pg/mL (33 fM) IgE was detected with this signaling method which was 1,000 times lower than that obtained with the conventional ELISA. The large clusters were much easier to purify after conjugation.

Free, unconjugated antibody molecules were removed after precipitating the clusters by brief centrifugation. On the contrary, the small NCs could not be purified from the free antibody and used as prepared. The free antibody could compete for the NCs-bound antibody in target binding and reduce signal intensity. The larger clusters exhibited longer shelf life owing to the lower surface activity. For the 44-nm clusters, aggregation and/or precipitation were not observed after storage of several months in water; while the small NCs could only be stable for up to one month. Moreover, sulfide is more resistant to oxidation than selenide, providing high stability to ZnS. Besides, the ZnS clusters contained the non-toxic chemical elements of Zn and S, had high stability in solutions, and were synthesized in an environmentally friendly manner at a low cost. All these features make CXAmp with ZnS clusters a highly sensitive, biocompatible, robust, and cost-effective tool for the detection of trace biomolecules. Advanced detection platforms such as microarray and microfluidic chips should further improve the performance of CXAmp with clusters by removing the diffusion obstacle. The high fluorescent signal readily detectible by conventional instruments shows the promise for CXAmp in portable point-of-care devices for biomarker detection.

Acknowledgement

The authors would like to acknowledge the financial support from National Science Foundation CAREER CHE-1057113, and the 2011-2012 grant from the Cancer Research Coordinating Committee provided to W. Zhong from UC Riverside. X. Han was partially supported by National Institute of Environmental Health Sciences Grant No.

1R21ES017870-01A1 awarded to W. Zhong. We are also very thankful to Dr. Tao Wu in Dr. Pingyun Feng's group (Department of Chemistry, UCR), for helping us to carry out the XRD and BET measurements.

Supporting Information

Supporting Information Available: XRD and BET results for characterization of NCCs; effect on fluorescence intensity from different microwave heating duration; comparison of the fluorescence amplification ratios among three cation release methods in three clusters; results from stability test of clusters stored in PBS or 0.02 M phosphate buffer; results from optimization of the amount of capturing antibody added, the amount of ZnS clusters used for detection; and the full range calibration curve for IgE detection using CXAmp in ZnS clusters. This material is available free of charge via the Internet at http://pubs.acs.org.

Figure and Table Captions

Table 1. BET surface area and average pore diameter obtained from nitrogen desorption for clusters of different diameters.

Figure 1. Zn release comparison in ZnS clusters of different diameters. The released Zn^{2+} was probed by 3 μM FluoZin-3. a) Nitric acid dissolution; b) Cation exchange reaction with 500 μM of Ag^{+} in 1 mM HEPES; c) Cation exchange reaction assisted with microwave irradiation for 2 minutes.

Figure 2. Binding of anti-hIgG labeled with ZnS clusters of different sizes to the surface of microtiter plate well that was completely coated with hIgG. The Zn^{2+} of ZnS clusters attached to the well was released through acid digestion and quantified by FluoZin-3. This Zn content was then used to calculate the total amount of ZnS clusters, assuming the clusters were solid particles when computed the total Zn in each cluster.

Figure 3. Schematic illustration of detection of IgE by streptavidin labeled ZnS cluster and biotinylated anti-IgE.

Figure 4. Human IgE detection performance. a) Comparison of IgE detection with two different ZnS-antibodies conjugates, i.e., ZnS-SB-antiIgE and ZnS-antiIgE. b). Performance comparison of IgE detection with CXAmp in ZnS clusters and ELISA. Signal amplification ratio was obtained by dividing the signal with the presence of IgE by the blank signal.

References

(1) Sahab, Z. J.; Semaan, S. M.; Sang, Q.-X. A. *Biomark. Insights* **2007**, 21-43.

(2) Ruge, D. R.; Dunning, F. M.; Piazza, T. M.; Molles, B. E.; Adler, M.; Zeytin, F. N.; Tucker, W. C. *Anal. Biochem.* **2011**, *411*, 200-209.

(3) Khan, M. R.; Anjum, F. M.; Din, A.; Hussain, S.; Shabbir, M. A.; Nadeem, M. *Food Agr. Immunol.* **2010**, *21*, 279-294.

(4) Rochelle, P. A.; Camper, A. K.; Nocker, A.; Burr, M. *Environ. Microbiol.* **2011**, 179-202.

(5) Dong, S.; Wang, B. *Electroanal.* **2002**, *14*, 7-16.

(6) Demchenko, A. P. *Anal. Biochem.* **2005**, *343*, 1-22.

(7) Steinkamp, T.; Karst, U. *Anal. Bioanal. Chem.* **2004**, *380*, 24-30.

(8) Khatkhatay, M. I.; Desal, M. *J. Immunoassay* **1999**, *20*, 151-183.

(9) Li, X.-M.; Yang, X.-Y.; Zhang, S.-S. *Trends Anal. Chem.* **2008**, *27*, 543-553.

(10) Shim, S.-Y.; Lim, D.-K.; Nam, J.-M. *Nanomedicine* **2008**, *3*, 215-232.

(11) Cao, Y. C.; Jin, R.; Mirkin, C. A. *Science* **2002**, *297*, 1536-1540.

(12) Liu, G.; Lin, Y. *Talanta* **2007**, *74*, 308-317.

(13) Penn, S. G.; He, L.; Natan, M. J. *Curr. Opin. Chem. Biol.* **2003**, *7*, 609-615.

(14) Edgar, R.; McKinstry, M.; Hwang, J.; Oppenheim, A. B.; Fekete, R. A.; Giulian, G.; Merril, C.; Nagashima, K.; Adhya, S. *Proc. Natl. Acad. Sci. USA* **2006**, *103*, 4841-4845.

(15) Medintz, I. L.; Uyeda, H. T.; Goldman, E. R.; Mattoussi, H. *Nat. Mater.* **2005**, *4*, 435-446.

(16) Wagner, M. K.; Li, F.; Li, J.; Li, X.-F.; Le, X. C. *Anal. Bioanal. Chem.* **2010**, *397*, 3213-3224.

(17) Kumar, R.; Maitra, A. N.; Patanjali, P. K.; Sharma, P. *Biomaterials* **2005**, *26*, 6743-6753.

(18) Li, Y.; Yip, W. T. *J. Am. Chem. Soc.* **2005**, *127*, 12756-12757.

(19) Gao, X. H.; Nie, S. M. *J. Phys. Chem. B* **2003**, *107*, 11575-11578.

(20) Lian, W.; Litherland, S. A.; Badrane, H.; Tan, W. H.; Wu, D. H.; Baker, H. V.; Gulig, P. A.; Lim, D. V.; Jin, S. G. *Anal. Biochem.* **2004**, *334*, 135-144.

(21) Yan, J. L.; Estevez, M. C.; Smith, J. E.; Wang, K. M.; He, X. X.; Wang, L.; Tan, W. H. *Nano Today* **2007**, *2*, 44-50.

(22) Goulko, A. A.; Li, F.; Le, X. C. *Trends Anal. Chem.* **2009**, *28*, 878-892.

(23) Ou, L.-J.; Liu, S.-J.; Chu, X.; Shen, G.-L.; Yu, R.-Q. *Anal. Chem.* **2009**, *81*, 9664-9673.

(24) Son, D. H.; Hughes, S. M.; Yin, Y. D.; Alivisatos, A. P. *Science* **2004**, *306*, 1009-1012.

(25) Li, J. S.; Schachermeyer, S.; Wang, Y.; Yin, Y. D.; Zhong, W. W. *Anal. Chem.* **2009**, *81*, 9723-9729.

(26) Yao, J. J.; Schachermeyer, S.; Yin, Y. D.; Zhong, W. W. *Anal. Chem.* **2011**, *83*, 402-408.

(27) Li, J. S.; Zhang, T. R.; Ge, H. P.; Yin, Y. D.; Zhong, W. W. *Angew. Chem. Intl. Ed.* **2009**, *48*, 1588-1591.

(28) Luther, J. M.; Zheng, H.; Sadtler, B.; Alivisatos, A. P. *J. Am. Chem. Soc.* **2009**, *131*, 16851-16857.

(29) Nguyen, T.-D.; Do, T.-O. *Langmuir* **2009**, *25*, 5322-5332.

(30) Wark, S. E.; Hsia, C.-H.; Son, D. H. *J. Am. Chem. Soc.* **2008**, *130*, 9550-9555.

(31) Yu, X.; Yu, J.; Cheng, B.; Huang, B. *Chem. A-Eur. J.* **2009**, *15*, 6731-6739.

(32) Liu, B.; Zeng, H. C. *Small* **2005**, *1*, 566-571.

(33) Cowles, C. L.; Zhu, X.; Publicover, N. G. *Analyst* **2011**, *136*, 2975-2980.

(34) Gee, K. R.; Zhou, Z.-L.; Qian, W.-J.; Kennedy, R. *J. Am. Chem. Soc.* **2002**, *124*, 776-778.

(35) Kubrakova, I. V.; Toropchenova, E. S. *Inorg. Mater.* **2008**, *44*, 1509-1519.

(36) Lidstrom, P.; Tierney, J.; Wathey, B.; Westman, J. *Tetrahedron* **2001**, *57*, 9225-9283.

(37) Qian, H. F.; Qiu, X.; Li, L.; Ren, J. C. *J. Phys. Chem. B* **2006**, *110*, 9034-9040.

(38) Sreeja, V.; Joy, P. A. *Mater. Res. Bull.* **2007**, *42*, 1570-1576.

(39) Korn, M. d. G. A.; Morte, E. S. d. B.; Batista dos Santos, D. C. M.; Castro, J. T.; Barbosa, J. T. P.; Teixeira, A. P.; Fernandes, A. P.; Welz, B.; Carvalho dos Santos, W. P.; Nunes dos Santos, E. B. G.; Korn, M. *Appl. Spectrosc. Rev.* **2008**, *43*, 67-92.

(40) Sneddon, J.; Hardaway, C.; Bobbadi, K.; Reddy, A. *Appl. Spectrosc. Rev.* **2006**, *41*, 1-14.

(41) Chen, C. M.; Chen, M.; Peng, Y. W.; Yu, H. W.; Chen, C. F. *Thin Solid Films* **2006**, *498*, 202-205.

(42) Stenberg, M.; Nygren, H. *J. Immunol. Methods* **1988**, *113*, 3-15.

(43) Tu, C. Y.; Kitamori, T.; Sawada, T.; Kimura, H.; Matsuzawa, S. *Anal. Chem.* **1993**, *65*, 3631-3635.

(44) Kemeny, D. M.; Richards, D.; Durnin, S.; Johannsson, A. *J. Immunol. Methods* **1989**, *120*, 251-258.

Figure 1.

a)

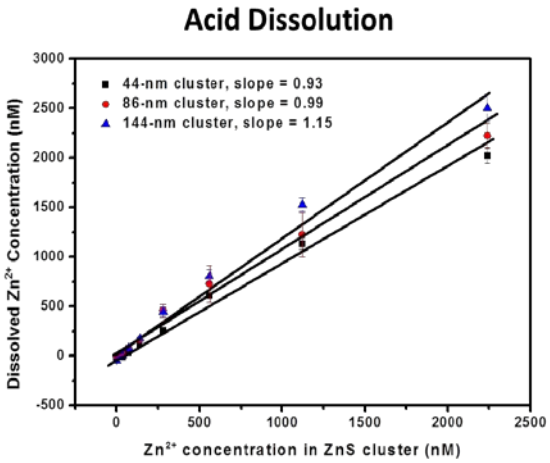
Acid Dissolution
44-nm cluster, slope = 0.93
86-nm cluster, slope = 0.99
144-nm cluster, slope = 1.15
Dissolved Zn2+ Concentration (nM)
Zn2+ concentration in ZnS cluster (nM)
3000
2500
2000
1500
1000
500
0
-500
0
500
1000
1500
2000
2500

b)

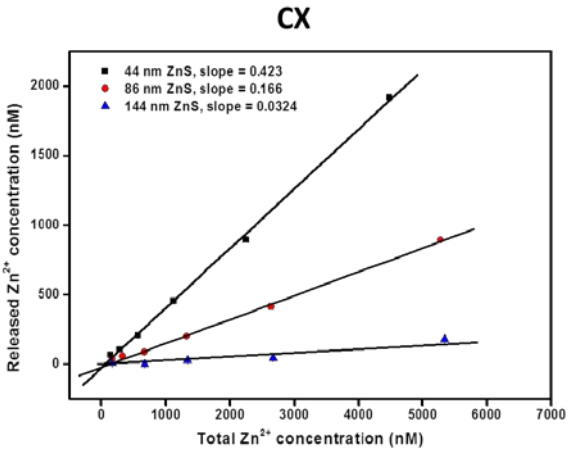
CX
44 nm ZnS, slope = 0.423
86 nm ZnS, slope = 0.166
144 nm ZnS, slope = 0.0324
Released Zn2+ concentration (nM)
Total Zn2+ concentration (nM)
2000
1500
1000
500
0
0
1000
2000
3000
4000
5000
6000
7000

c)

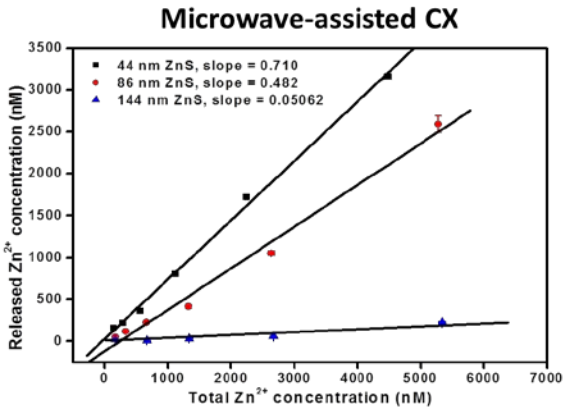
Microwave-assisted CX
44 nm ZnS, slope = 0.710
86 nm ZnS, slope = 0.482
144 nm ZnS, slope = 0.05062
Released Zn2+ concentration (nM)
Total Zn2+ concentration (nM)
0
500
1000
1500
2000
2500
3000
3500
0
1000
2000
3000
4000
5000
6000
7000

Figure 2.

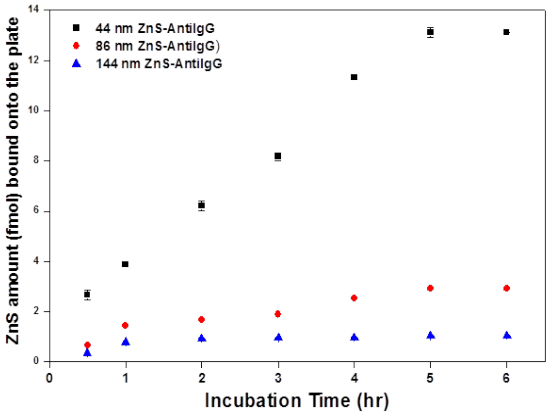
44 nm ZnS-AntiIgG
86 nm ZnS-AntiIgG)
144 nm ZnS-AntiIgG
ZnS amount (fmol) bound onto the plate
Incubation Time (hr)
0
2
4
6
8
10
12
14
0
1
2
3
4
5
6

Figure 3.

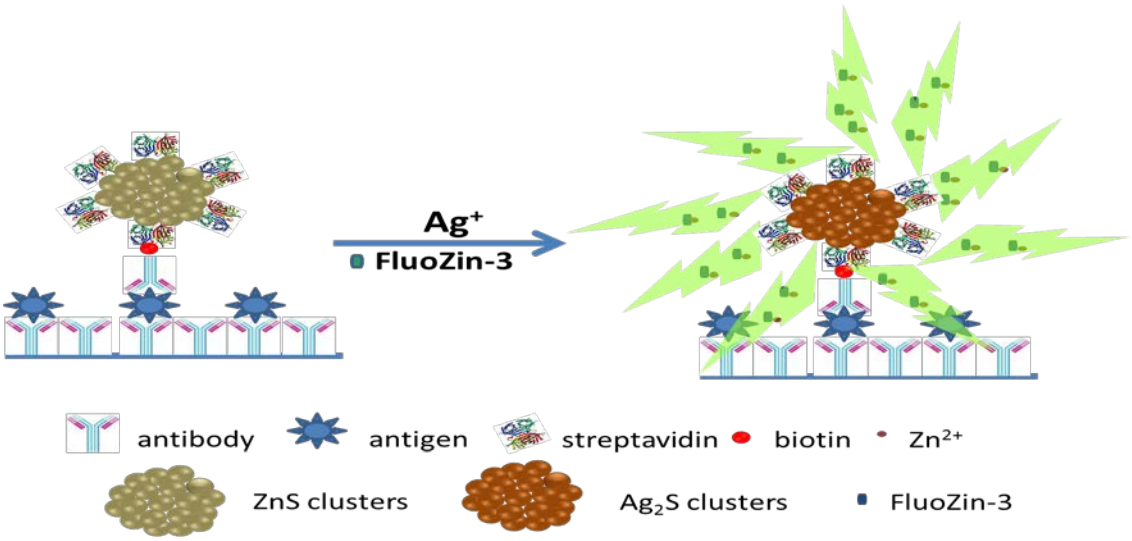
Ag+
FluoZin-3
antibody
antigen
streptavidin
biotin
Zn2+
ZnS clusters
Ag2S clusters
FluoZin-3

Figure 4.

a)

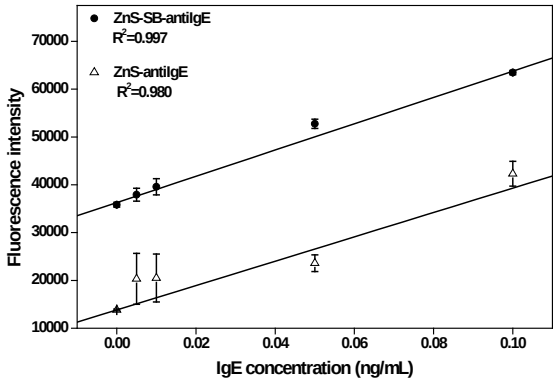
ZnS-SB-antiIgE
R²=0.997
ZnS-antiIgE
R²=0.980
Fluorescence intensity
70000
60000
50000
40000
30000
20000
10000
0.00
0.02
0.04
0.06
0.08
0.10
IgE concentration (ng/mL)

b)

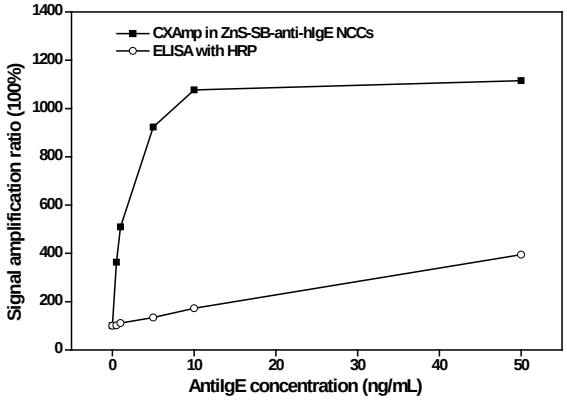
CXAmp in ZnS-SB-anti-hIgE NCCs
ELISA with HRP
Signal amplification ratio (100%)
1400
1200
1000
800
600
400
200
0
0
10
20
30
40
50
AntiIgE concentration (ng/mL)

Table of Contents